ACS OMEGA

Open Access



http://pubs.acs.org/journal/acsodf

Article

# SI/II Pocket of Ras: An Opportunity for a Once "Undruggable" Target

Tanos C. C. França,[⊥] Michael Maddalena,[⊥] Imène Kouidmi, Yann Ayotte, Salim T. Islam, and Steven R. LaPlante*

Cite This: *ACS Omega* 2025, 10, 9463−9473

Read Online

ACCESS | Metrics & More | Article Recommendations | Supporting Information

**ABSTRACT:** Mutations on the Ras-family of small GTPases are among the most common molecular oncogenic drivers, with the HRas isoform being primarily associated with head-and-neck and genito-urinary cancers. Although once considered "undruggable," recent efforts have identified a structurally conserved surface pocket in the Ras family, designated the SI/II pocket, situated near the binding site of the guanidine exchange factor (GEF) SOS1. The SI/II pocket may represent a potential target site for a pan-Ras drug. A crystal structure representing the native state of GDP-bound HRas$^{G12V}$ was generated to characterize the topology of the SI/II pocket. This native-state structure was employed, together with the published structure of GppNHp-bound HRas$^{G12V}$ in state 1 (PDB ID: 4EFM), as a base for further molecular dynamics simulations exploring the conformational dynamics of the SI/II pocket via four generated synthetic HRas model structures. Our results show that the SI/II pocket is natively inaccessible in GDP-bound HRas yet becomes accessible in state 1 GppNHp-bound HRas systems, an effect that seems to be more evident in the mutated enzyme. This points to the GTP-bound state as a most promising target for Ras inhibitors directed at the SI/II pocket. Occlusion of the SI/II pocket is dictated by the spatial position of the α2 α helix in relation to the protein core, with α2 residue Y71 acting as a "tyrosine toggle" capable of restricting the pocket access.

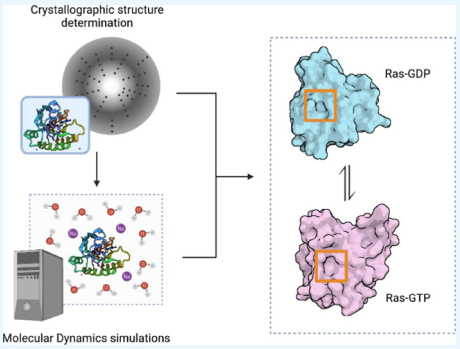


## INTRODUCTION

The rat sarcoma (Ras) subfamily of small GTPases is a group of molecular switches responsible for regulating signal transduction in pathways involved in cell proliferation and growth, metabolism, and apoptosis.[1] Clinically observed Ras mutants involve gain-of-function mutations, which induce the breakdown of tight regulation in cellular pathways due to abnormal rates of Ras-mediated signaling, promoting tumorigenesis.[2] Ras mutations are frequently observed in tumors and are estimated to be present in approximately 19% of all cancers presenting in the clinic.[3] Classical human Ras GTPases are divided into three isoforms: KRas, NRas, and HRas, with each isoform predominantly associated with distinct cancer types when mutated.[4] HRas is the less common (and less studied) isoform observed in cancers. However, it represents the most common mutated isoform identified in Ras-associated head-and-neck and genito-urinary cancers.[3] It is, for this reason, the primary target of our research efforts toward discovering new anticancer drugs[5]

All classical Ras isoforms display intrinsic hydrolase activity, switching between the "active" GTP-bound state, capable of activating downstream signaling effectors, and the inert "inactive" GDP-bound state (Figure 1).[6] All known oncogenic point mutations within Ras disrupt normal switching kinetics by directly impacting intrinsic hydrolase activity or disrupting interactions with proteins involved in assisting nucleotide hydrolysis and exchange (RasGAP/RasGEF).[7] Mutations in Ras disrupting intrinsic hydrolase activity are primarily observed

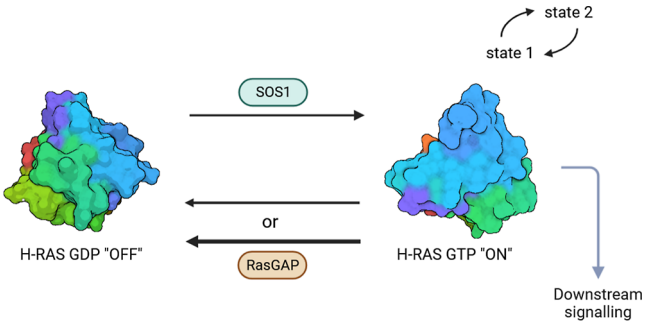


**Figure 1.** Functional overview of Ras signaling. A simple mechanistic overview of the switching behavior of HRas, alternating between the biologically active GTP-bound state ("on") and the inactive GDP-bound state ("off"). RasGEF (SOS1) and RasGAP assisting nucleotide exchange and hydrolysis are depicted. Relative nucleotide hydrolysis and exchange rates are represented, connecting either state of Ras.

at residues G12, G13 and Q61;[4] mutations within the functional P-loop region of Ras (residues G10-S17), such as G12V in

Received: November 18, 2024
Revised: January 19, 2025
Accepted: February 5, 2025
Published: February 28, 2025





https://doi.org/10.1021/acsomega.4c10493
*ACS Omega* 2025, 10, 9463−9473

HRas, unsettle GTPase activity by sterically inhibiting transition state geometry during hydrolysis.[8,9] Additionally, glycine substitution at residue 12 for an amino acid residue containing a bulkier side chain (such as valine) disrupts interactions with RasGAP , decreasing GTPase activity.[8,10] Ras point mutations may have functional effects on both the GDP-bound and GTP-bound forms of Ras.[11]

GTP-bound Ras is found in one of two interconverting conformational states (Figure 1), with state 1 demonstrating a low intrinsic hydrolysis rate as well as reduced interactions with downstream effectors, and state 2 demonstrating higher intrinsic hydrolysis rates and an increased affinity for downstream effectors.[12] Common Ras point mutations can skew the population of GTP-bound Ras toward either of these states. The G12V mutation heavily favors state 1 over state 2 with respect to kinetic parameters.[13]

Two flexible loop regions situated within the effector G-domain (residues M1-H166) of HRas have been identified as interaction sites for accessory proteins and downstream effectors alike: switch I (residues Y32−Y40) and switch II (residues D57-G75).[14] Both switch regions collectively comprise a surface critical to downstream signal transduction initiated through protein−protein interactions, assuming various spatial orientations based on the nucleotide bound and the subsequent conformational state of the protein.[15] Notably, the first 86 residues of the protein are highly conserved across all classical Ras isoforms, a section within which both switch regions are found.[16] These 86 N-terminal conserved residues form a protein region referred to as "lobe 1".[17] A structurally conserved pocket, designated as the SI/II pocket, has been identified on the surface of the protein within lobe 1; this pocket is lined by lipophilic residues comprising both switch regions (S39, Q70, Y71, T74), as well as several other surface and core residues found within lobe 1 (K5, D54, L56).[18] The namesake for the SI/II pocket is derived from its proximity to the RasGEF-type protein Son of Sevenless (SOS1) binding site, located near the interface of both switch regions.[19] As the SI/II pocket is comprised uniquely of amino acid residues found within lobe 1, it is present in all classical isoforms of Ras and maintains its relative geometry, rendering it an attractive site for the design of a potential pan mutant and pan-isoform Ras drug which has yet to be reported in the literature.[20] Native accessibility of the SI/II pocket to a small-molecule binding directly depends on the orientation of $\alpha$2, a right-hand $\alpha$ helix motif located near the C-terminal end of the switch II region. The orientation of Y71, a critical residue within $\alpha$2, is directly related to the native accessibility of the SI/II pocket; Y71 functions as a "tyrosine toggle", a gate barrier arm controlling access to the interior surface of the SI/II pocket.

Several crystal structures have been submitted to the worldwide Protein Databank (PDB) (www.rcsb.org) depicting small-molecule compounds binding to the SI/II pocket across all classical Ras isoforms (e.g., PDB IDs 4DSO, 6ZL3, 4EPY, 6GJ8), suggesting that this pocket can indeed be targeted by a small molecule drug.[18,20−22] These concept drugs share common core structural features: an indole ring or benzimidazole at their core, which functions as an anchor lodging the compound to the inside surface of the SI/II pocket via hydrophobic interactions.[23] Previous results in the literature suggest that rational drug design targeting the SI/II pocket is possible for both the GDP and GTP-bound forms of Ras.[22]

Here, we present a complete crystal structure of the GDP-bound mutant $HRas^{G12V}$ G-domain (PDB ID: 7TAM) with both switch regions fully modeled. Using this structure, the experimental structure of GppNHp-bound (GNP) mutant $HRas^{G12V}$ (PDB ID: 4EFM), as well as four synthetic HRas models generated *in-house*, we also present molecular dynamics (MD) simulations detailing the behavior of the SI/II pocket, resulting from conformational changes occurring in the transition between the "inactive" and "active" states of Ras. These simulations provide insight into the behavior of the SI/II pocket in both the GDP and simulated GppNHp forms of $HRas^{G12V}$ and $HRas^{Wild}$. Due to the conserved nature of the SI/II pocket, the results of our simulations can contribute to a better understanding of the behavior of the SI/II pocket. By characterizing the conformational dynamics of the SI/II pocket, we aim to supplement general understanding of this target to assist structure-based drug design efforts in a protein of sustained oncologic interest.

## METHODOLOGY

**Protein Purification.** The G-domain of $HRas^{G12V}$ (residues 1-166) was expressed witha poly-histidine tag in *Escherichia coli* BL21(DE3) competent cells (Thermo Fischer Scientific, EC0114) from a pET28a(+) (RRID: Addgene_26094) plasmid vector transfected via heat shock. Transformed *E. coli* cells were grown to saturation for 18 h overnight in LB media with 1% Kanamycin added (350 rpm, 37 °C) in a 250 mL ultra-yield flask (Thomson Scientific, 50-996-059). The overnight *E. coli* culture was diluted into fresh LB + 1% Kanamycin in 1.5 L Ultra-Yield flasks at a 1:10 volume ratio. Four Ultra-Yield flasks containing a total of 2 L of LB + 1% Kanamycin*E. coli* bacterial culture were incubated with shaking (300 rpm, 37 °C) until the cultures reached an optical density at 600 nm of 3.5 . One mM IPTG was added to*E. coli* cell cultures to induce protein production for 18 h in an incubator with shaking (180 rpm, 25 °C). Cells were sedimented via centrifugation (20,000 g,30 min, 4 °C), resuspended in buffer (50 mM Tris−HCl, 500 mM NaCl and 1 mM TCEP at pH 8) and lysed via sonication. Cell lysate was centrifuged and filtered using a 0.45 $\mu$m PVDF filter membrane (EMD Millipore, HVLP04700). Expressed $HRas^{G12V}$ was separated from cellular proteins via immobilization on a 5 mL HisTrap FF histidine affinity column (Cytiva, 17525501), then eluted with increasing concentrations of imidazole. $HRas^{G12V}$ eluate was cleaved overnight via exposition to recombinant TEV protease in buffer solution +2 mM TCEP at a 10:1 TEV/HRas molar ratio, and then processed through reversed immobilized metal affinity chromatography (IMAC). Endogenous nucleotide was exchanged for GDP (Sigma-Aldrich, G7127) via a Ras nucleotide exchange protocol interpreted from Maurer et al.[21] The resulting $HRas^{G12V}$-GDP product was further purified via size-exclusion chromatography using a HiLoad 26/600 Superdex 75 pg column (Cytiva, 28989334); purified $HRas^{G12V}$-GDP in solution was concentrated to 14 mg/mL by centrifugation using a 3.000 MWCO Ultra-15 filter unit (EMD Millipore, UFC900324, 20,000 g, 30 min, 4 °C).

**Crystallization and Cryoprotection.** GDP-bound $HRas^{G12V}$ crystals were grown at ambient room temperature (295.15 K) via the hanging drop vapor diffusion method; 2 $\mu$L drops were exposed to a reservoir solution composed of 29% PEG 3350, 0.2 M calcium chloride dihydrate and 0.1 M Tris hydrochloride at pH 8. Hanging drops consisted of a 1:1 mixture of purified GDP-bound $HRas^{G12V}$ and reservoir solution. Crystals were recovered using 20 $\mu$m Mounted CryoLoops (Hampton Research, HR4-955) and soaked in a cryoprotectant solution (25% PEG 4000, 2 M calcium chloride dihydrate, 15%


https://doi.org/10.1021/acsomega.4c10493
ACS Omega 2025, 10, 9463−9473

glycerol) before being expedited to the Canadian Light Source complex (CLS).

**Data Collection, Processing and PDB Deposition.** Data collection was performed at the CLS complex using the CMCF-BM (08B1) beamline. $HRas^{G12V}$-GDP crystals were exposed to the X-ray beamline at a wavelength of 1.5212 Å at 100 K. Diffraction maps were collected using a Pixel Dectris Pilatus3 S 6 M detector. Diffraction data were processed using autoPROC (incl. XDS/XSCALE Staraniso, Pointless, Aimless) and recovered through the CLS MxDc interface.[24] Molecular replacement was performed in PHENIX using a deposited $HRas^{G12S}$ GDP structure (PDB ID: 6MQT) as a starting model.[25] Refinement was performed at 1.87 Å using the phenix.refine module, with manual corrections performed in CCP4 WinCoot.[26] The refined crystal structure of $HRas^{G12V}$ GDP was deposited in the RCSB PDB (www.rcsb.org) under the accession code7TAM. Statistics for initial diffraction data and refinement data for 7TAM were gathered using both PHENIX and the MolProbity toolkit (RRID: SCR_014226) (Table S1).[24,27] Ramachandran plots (Figure S1) were generated using the Ramplot python module v.1.0.4. Polder OMIT maps comprising all residues in Ras lobe 1 (residues 1−86) were generated for GDP-bound $HRas^{G12V}$ (PDB ID: 7TAM) and GppNHp-bound $HRas^{G12V}$ (PDB ID: 4EFM) (Figure S6) using PHENIX. Per-residue polder OMIT maps for 7TAM SI/SII pocket residues were generated using PHENIX.

**Molecular Dynamics Simulations.** MD simulations were performed using the crystal structures of GDP-bound $HRas^{G12V}$ (PDB ID: 7TAM) and GppNHp-bound $HRas^{G12V}$ (PDB ID: 4EFM) plus four synthetic models derived from these experimental structures, constructed using the builder module of the Molecular Operational Environment [MOE (https://www.chemcomp.com/Products.htm)] software. Model 1 was generated by replacing one of the −O atoms of the $\beta$-$PO_4$ group of GDP in 7TAM with a $-NPO_3$ group to create a simulated structure of GppNHp-bound $HRas^{G12V}$ with an occluded SI/II pocket. Model 2 was generated by replacing the $-NPO_3$ group of GppNHp in 4EFM with a −O atom to create a simulated structure of GDP-bound $HRas^{G12V}$ without SI/II pocket occlusion. Models 3 and 4 represent $HRas^{wild}$ in the GTP and GDP-bound forms and were created by reversing the mutation G12V and changing GppNHp to GTP.

**Table 1. Energy Thresholds Used to Generate the Fingerprints**

| Type of interaction | | Weak (kcal.mol$^{-1}$) | Strong (kcal.mol$^{-1}$) |
|---|---|---|---|
| Side chain | H-donor | 0.5 | 1.5 |
| | H-acceptor | 0.5 | 1.5 |
| Backbone | H-donor | 0.5 | 1.5 |
| | H-acceptor | 0.5 | 1.5 |
| Solvent | H-donor | 0.5 | 1.5 |
| | H-acceptor | 0.5 | 1.5 |
| Ionic attraction | | 0.5 | 3.5 |
| Metal ligation | | 0.5 | 3.5 |
| Arene attraction | | 0.5 | 1.0 |

The .pdb files of 7TAM,4EFM and the synthetic models were first opened in the main window of MOE (https://www.chemcomp.com/Products.htm) and optimized with the *quick-prep* tool to achieve the proper bond lengths, angles and charges compatible with the physiological environment. Each file was then prepared for simulation using the compute/simulations/dynamics module of MOE (https://www.chemcomp.com/Products.htm). The simulations were performed in triplicate, at 310 K, using the AMBER10:EHT[28] force field and the NAMD software[29] with cutoff = 10 for electrostatics and between 8 and 10 for VdW interactions. This force field has been successfully used by our research group to simulate biological systems in prior studies;[30] it is well-characterized in the literature and is thus the standard force field used by MOE (https://www.chemcomp.com/Products.htm) for this purpose.[31] Each protein was centered in a cubic box containing between 8,000 and 10,000 water molecules neutralized with $Na^+$ ions. Before the 1 $\mu$s simulation production step, each system was submitted to a 10 ps energy minimization followed by 100 ps of *NPT* and 200 ps of *NVT* under Langevin dynamics parameters.[32] The trajectories obtained were analyzed using the md_analysis tool and the database viewer (DBV) menu of MOE (https://www.chemcomp.com/Products.htm), while plots of MD results were created using GraphPad PRISM (RRID: SCR_002798) (https://www.graphpad.com). Movies of the MD simulations were generated using the Visual Molecular Dynamics (VMD) software[33] and the H-bonds were calculated following the standard VMD[33] distance/angle criteria of 3.5 Å and 20°, respectively. The initial volume of the SI/II pocket was determined using the PyVOL[34] plugin of PyMOL[35] and monitored through plots of Solvent Accessible Surface Area (SASA) from the md_analysis tool of MOE (https://www.chemcomp.com/Products.htm).

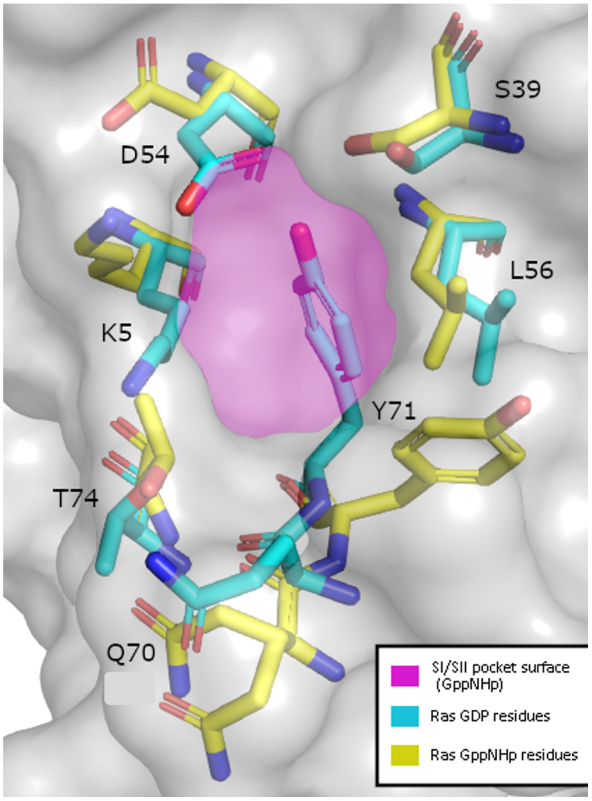


**Figure 2.** Spatial orientation of amino acid residues comprising the SI/II pocket in the GDP-bound (cyan - PDB ID: 7TAM) and GppNHp-bound (yellow - PDB ID: 4EFM) forms of $HRas^{G12V}$. The accessible pocket surface, as observed in the GppNHp-bound form, is highlighted (magenta). In the GDP-bound form the pocket surface is occluded by residues K5, D54 and Y71 (cyan).



https://doi.org/10.1021/acsomega.4c10493
ACS Omega 2025, 10, 9463−9473

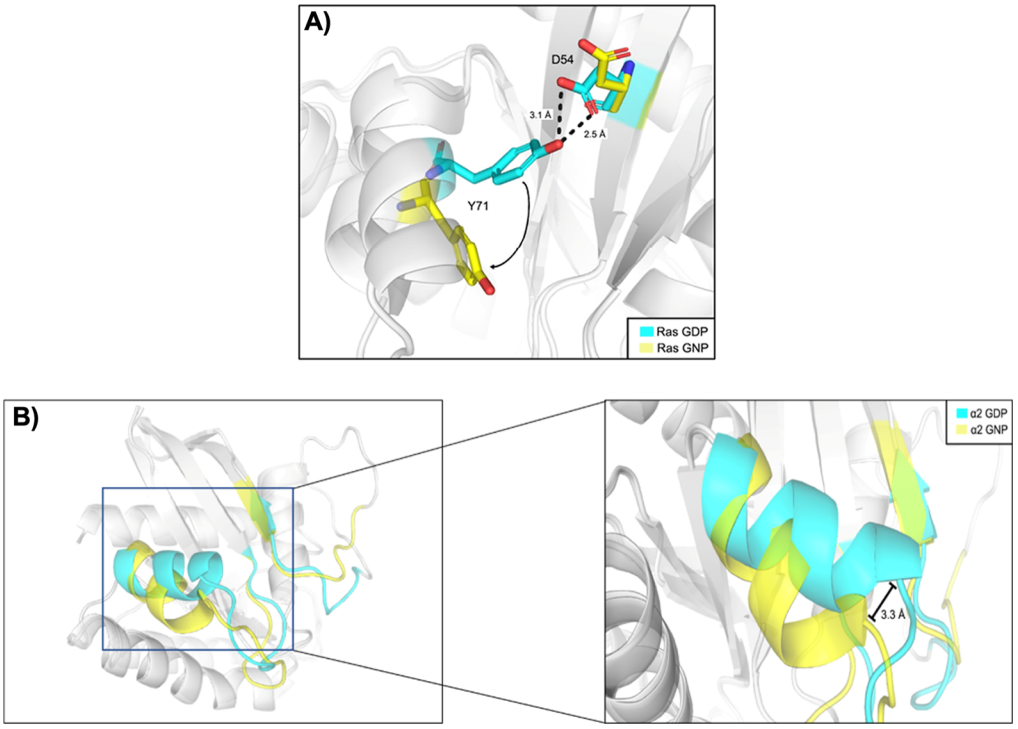


**Figure 3.** Conformational dynamics of the Ras switch regions and residue Y71 in the GDP-bound (cyan, PDB ID: 7TAM) and GppNHp-bound forms (yellow, —PDB ID: 4EFM) of HRas$^{G12V}$. (A) Relative orientation of D54 and Y71 . H-bond interactions and the Euclidean distances between the terminal hydroxyl of Y71 and the terminal carbonyl of D54, are evidenced. (B) The relative orientation of switches I and II regions . The position of the terminal $\alpha$2 helix within switch II is evidenced.

**Fingerprint Analysis.** In order to contribute for the design of a potential pan-Ras binder to the SI/II pocket, the protein ligand interaction fingerprint (PLIF) application of MOE (https://www.chemcomp.com/index.htm) was used to map the most relevant residues for pan-Ras activity. All the experimental structures of Ras bearing ligands in the SI/II pocket available in the PDB (www.rcsb.org) were downloaded into a databank. This Ras-ligand structure databank was further used to prepare and generate the fingerprints using the PLIF setup panel with weak and strong energy thresholds for the nine types of protein−ligand interactions normally observed in fingerprints, set as indicated in Table 1. The resulting fingerprints were compiled in a barcode plot.

## RESULTS

**Crystallographic Structures.** The GDP-bound form of HRas$^{G12V}$ (PDB ID: 7TAM) presents a glycine-to-valine substitution at residue 12, adopting a unique conformation within the P-loop (residues 10−17) impacting nucleotide binding without altering the overall GTPase fold. Consistent with other GDP-bound forms of Ras, the switch I and switch II regions are in an inactive conformation, held in proximity by hydrogen bonds (H-bonds) and van der Waals interactions between residues T35-Y40 and D57-G60 respectively.

In the GDP-bound form of HRas$^{G12V}$ (PDB ID: 7TAM), residue Y71 occupies a central position in the SI/II pocket, bordered by residues K5, S37, D54, L56, Q70 and T74 (Figure 2), while in the GppNHp-bound form in state 1 (PDB ID: 4EFM) Y71 is resigned to the border of the SI/II pocket (Figure 2). The experimental structure of HRas$^{Wild}$ GppNHp-bound in state 2 (PDB ID: 5B2Z) also presents Y71 in the same configuration as 4EFM. The native conformation of residue Y71 in the GDP-bound form of HRas$^{G12V}$ shields the hydrophobic interior of the SI/II pocket, impeding access to the pocket. This native conformation is maintained via 2.5 and 3.1 Å H-bond interactions between residues D54 and Y71 (Figure 3A). Our study of MD simulations on the GDP-bound form of HRas also revealed the possibility of a rare, transient H-bond interaction between Y71−OH and the protein backbone carbonyl of D54 (D54-O).

In the GppNHp-bound form of HRas$^{G12V}$ (PDB ID: 4EFM), supplemental contacts between the $\gamma$-phosphate of GppNHp create additional steric interactions with residues preceding the switch II region; these interactions consequently displace switch II and deviate the position of the $\alpha$2 helix harboring residue Y71 by 3.3 Å at its N-terminal base (Figure 3B). Structural differences within the $\alpha$2 helix region (residues 67−75) are central to changes in the accessibility of the SI/II pocket between the GppNHp and GDP-bound forms of HRas$^{G12V}$. In the GppNHp-bound form, deviation of $\alpha$2 affects the position of the $\alpha$ carbon of Y71, which is now situated 2.0 Å further relative to the $\alpha$ carbon of D54. This 2.0 Å deviation causes the side chain of Y71 to "flip" its orientation via a clockwise rotation relative to the backbone (Figure 3A). As a result, the H-bond interactions between Y71 and D54 are impeded. The loss of these H-bond interactions leads Y71 to stabilize in the "flipped" orientation (Figure 3A); the side chain of Y71 then interacts with side chain carbons in residue M67, a spatial neighbor situated one preceding turn in the $\alpha$2 helix at position i-4. In the "flipped" orientation, Y71 no longer occupies a central position in the SI/II pocket, exposing its hydrophobic interior to the solvent (Figure 2); this phenomenon is observable in both states 1 and 2 of GppNHp-bound Ras (see PDB IDs: 4EFM and 5B2Z).

*MD Simulations.* Long MD simulations (1 $\mu$s) were first performed on the crystallographic structures of GDP-bound


https://doi.org/10.1021/acsomega.4c10493
ACS Omega 2025, 10, 9463−9473

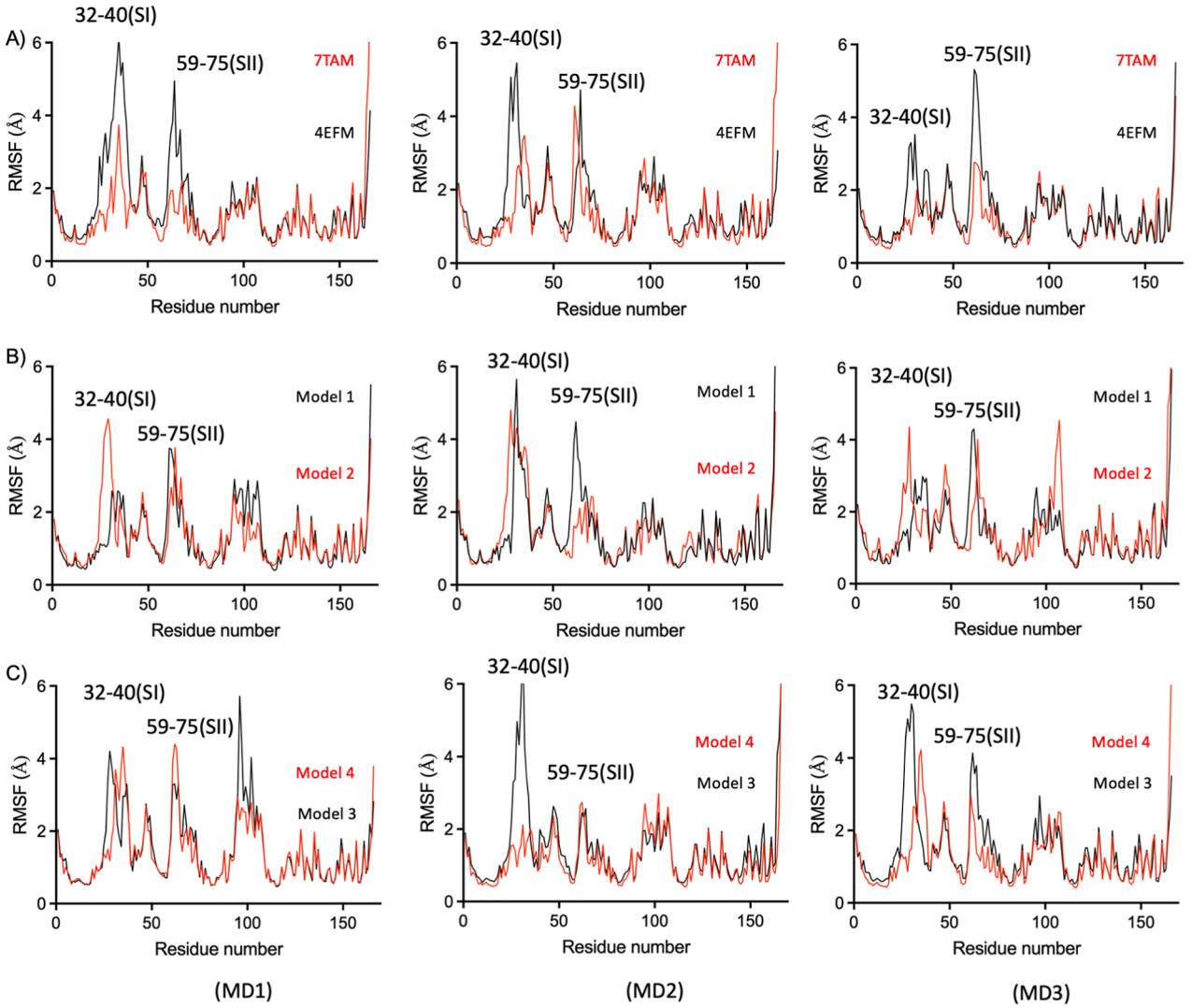


**Figure 4.** Plots of RMSF after 1 $\mu$s of MD simulations. (A) 7TAM and 4EFM (B) Models 1 and 2 (C) Models 3 and 4.

HRas$^{G12V}$ (PDB ID: 7TAM—SI/II pocket occluded) and GppNHp-bound HRas$^{G12V}$ (PDB ID: 4EFM—SI/II pocket accessible) to verify the accessibility of the SI/II pocket over time. These simulations were also performed to validate the general conformational state of both experimental structures. Additionally, four synthetic models were constructed from both experimental crystal structures (7TAM, 4EFM) with the following modifications: (1) GDP-bound HRas$^{G12V}$ (7TAM) modified to GppNHp-bound (referred to as "Model 1"); (2) GppNHp-bound HRas$^{G12V}$ (4EFM) modified to GDP-bound HRas$^{G12V}$ (referred to as "Model 2"); 3) GppNHp-bound HRas$^{G12V}$ (4EFM) mutated to GTP-bound HRas$^{Wild}$ (referred to as "Model 3"); (4) GDP-bound HRas$^{G12V}$ (7TAM) mutated to GDP-bound HRas$^{Wild}$ (referred to as "Model 4"). Models 1−4 were also submitted to 1 $\mu$s-long MD simulations. All simulations were performed to investigate the conformational behavior of the SI/II pocket relative to the type of nucleotide bound to the protein (GDP or GppNHp/GTP). Using data inferred from MD simulations, plots were generated to represent the variation of total system energy (Figure S1), Root Mean Square Deviation (RMSD) (Figure S2) and Root Mean Square Fluctuation (RMSF) for all MD simulations (Figure 4). The dynamic behavior of residues D54 and Y71 are evidenced in Supplementary Movies S1−S6 and in Euclidean distance variation violin plots between the terminal hydroxyl of Y71 and the C$\gamma$ atom of D54 (Figure 5). The initial volume of the SI/II pocket was determined to be 102 Å; the plots of SASA variation during the MD simulations are shown in Figure S3. The small variations in SASA over time point to a preservation of the pocket geometry for the duration of the simulation in all systems. Tables 2 and 3 present, respectively, the prevalence of H-bonds formed over time between the bound nucleotide (GDP or GppNHp/GTP) and HRas nucleotide pocket residues, as well as between Tyr71 and other HRas residues. H-bond prevalence is listed as a percentage.

**Fingerprint Analysis.** The bar code plot in Figure 6 shows that the most frequent interactions with residues of the SI/II pocket happen with D54 (H-bonds and ionic) followed by S39 (H-bonds), K5 (H-bond and arene), L56 (only arene), T74 (H-bonds and arene) and Q70 (H-bonds). Among residues that do not belong to the SI/II pocket the most frequent were E37 (H-bonds and arene), E3 (H-bond and ionic) and D38 (H-bond and ionic).

## DISCUSSION

The crystallographic data collected indicates that the GTP-bound form of Ras (state 1) may be the ideal drug target over the



https://doi.org/10.1021/acsomega.4c10493
ACS Omega 2025, 10, 9463−9473

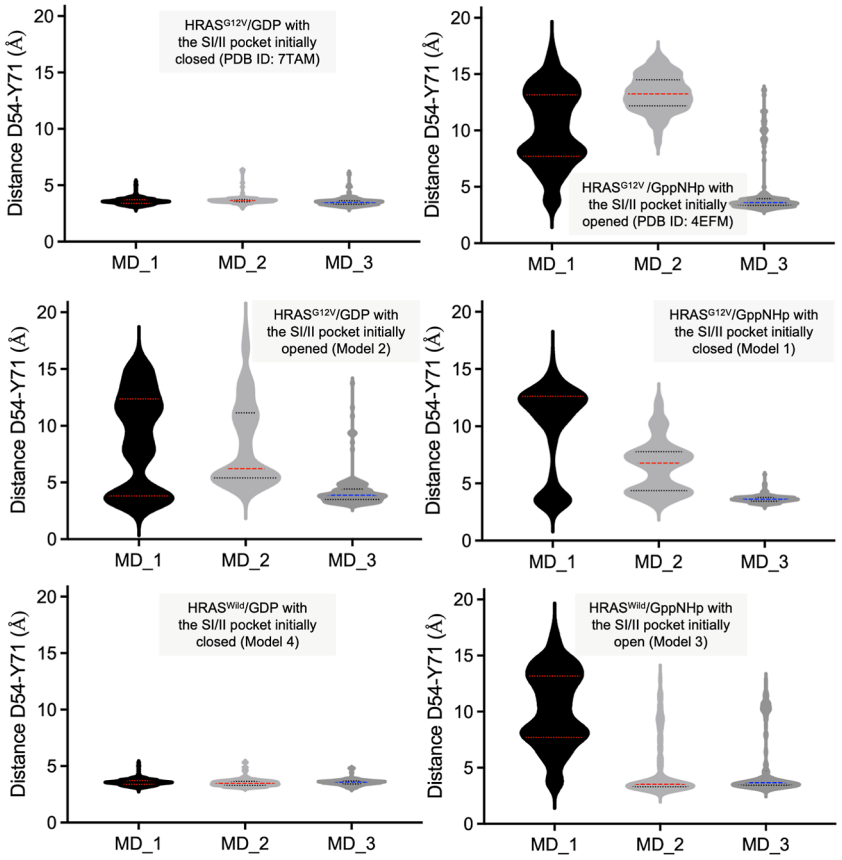


**Figure 5.** Violin plots of the Euclidian distance variation between residues D54 and Y71 over the duration of each MD simulation. The initial state of the SI/II pocket accessibility ("open" or "closed") is reported for each system.

GDP-bound form for any given small molecule compound designed to bind the SI/II pocket. While the SI/II pocket is natively accessible in the GppNHp-bound form HRas model, it is occluded by pocket amino acid residues forming H-bond interactions in the GDP-bound form of the protein, as shown in Figure 2. A compound designed to bind the "state 1" of GTP-bound Ras isoforms may act physiologically by decreasing mutation-amplified signal transduction, achieved by blocking the transition toward the more signal transduction-competent GTP-bound "state 2".[36] Due to the proximity of the SI/II pocket to the binding interfaces of downstream effector proteins, a SI/II-targeted compound may also double as a contact inhibitor between Ras and downstream effectors.[37]

Several Ras drug candidates in the literature contradict this conclusion: numerous crystal structures in the PDB database (www.rcsb.org) present evidence for several small molecule compounds binding to the SI/II pocket in the GDP-bound form of Ras. This suggests a possible induced fit of the ligand into the SI/II pocket. However, in several cases, these Ras-ligand crystal structures must be interpreted with caution: instances are present in published structures across the PDB (www.rcsb.org) where the target compound is not bound within the SI/II pocket strictly via ligand-target monomer protein interactions. Instead, the compounds presented appear dependent on crystal contacts from another Ras molecule instance in a neighboring asymmetrical unit (ASU) to "trap" these compounds within the SI/II pocket during crystallization (e.g., PDB IDs: 4DSU, 4EPY, 6GJ8, 6ZL3). These structures presenting "trapped" compounds do not discredit the status of the presented compounds as true binders of Ras, as several studies argue that Ras does dimerize *in vivo*; thus, targeting Ras as a dimer rather than as a monomer may constitute a valid but not yet thoroughly explored mechanism. Compounds designed to bind Ras dimers have already been reported in the literature.[38] Additional study is required to substantiate the biological significance of these findings, given the controversial nature of the Ras dimer hypothesis.[39] We recommend concurrently using complementary techniques, such as MD simulations and HSQC NMR, to confirm the binding mode and behavior for a small molecules within the SI/II pocket and to further investigate binding to potential Ras dimers. X-ray crystallography experimentation remains relevant in Ras SI/II-pocket targeted drug design, as crystallographic data can assist development by generating a protein−ligand structure to be used as a starting point for modeling or as cross-validation for other methods.

The nucleotide analog GppNHp was initially chosen for prior crystallographic experimentation due to its widespread presence in published Ras structures (e.g., PDB IDs: 1XCM, 4G0N, 6GOD, 6E6H) and relative availability. Using GppNHp or another nonhydrolyzable nucleotide analog are paramount in obtaining an "active" Ras crystal structure, as the combination of the self-hydrolyzing activity of Ras and the long timeframes required for crystal formation render the use of GTP untenable within the crystallographic pipeline. As our work seeks to inform future structure-based drug design efforts linking multiple methodological strategies, often including X-ray crystallography, GppNHp use was extended to MD simulations as a consistent reference for dynamic analysis.

The plots of variation of total energy point toward immediate system stabilization near the first nanosecond of simulation in all


https://doi.org/10.1021/acsomega.4c10493
ACS Omega 2025, 10, 9463−9473

Table 2. H-Bonds Formed between GDP or GppNHp/GTP and HRas during the MD Simulations[a]

| System | Interacting protein residues | |
|---|---|---|
| | Acceptor | Donor |
| 7TAM (GDP) | V29 (35.82%), D30 (75.13%), D119 (157.21%) | G15 (23.88%), K16 (112.94%), S17 (28.36%), A18 (44.78%), K147 (21.89%) |
| 4EFM (GppNHp) | G13 (38.81%), D30 (19.90%), D119 (157.21%) | G13 (57.21%), K16 (97.51%), S17 (30.35%), A18 (24.88%), K147 (48.26%) |
| Model 1 (GppNHp) | G13 (29.85%), V29 (30.35%), D30 (27.36%), D119 (158.71%) | G13 (58.71%), G15 (15.92%), K16 (125.37%), S17 (48.76%),A18 (41.79%), N116 (11.94%),K147 (41.80%) |
| Model 2 (GDP) | D33 (78.61%), D119 (136.82%) | K16 (102.98%), S17 (71.74%), K147 (34.33%) |
| Model 3 (GTP) | G13 (11.44%), D30 (21.39%), E31 (22.89%), D119 (154.23%) | G13 (43.78%), G15 (20.40%), K16 (103.98%), S17 (36.82%), A18 (39.30%), K147 (35.32%) |
| Model 4 (GDP) | V29 (26.87%), D30 (51.24%), D119 (171.14%) | G13 (29.35%), G15 (25.37%), K16 (114.43%), S17 (32.84%), A18 (41.79%), K147 (33.33%) |

[a]Only the residues forming H-bonds with the ligand for over 10% of the simulated time are shown. Values above 100% indicate that the ligand has formed more than one H-bond with that residue.

systems, with an average slightly above −80,000 kcal.mol$^{-1}$ for systems with an occluded SI/II pocket and below this value for the systems with an accessible SI/II pocket (Figure S1). The RMSD plots do not present spatial position deviations over 1.50 and 4.50 Å for ligand and protein, respectively (Figure S2). Additionally, the RMSF plots demonstrate that the 3D spatial position of most amino acids in the protein fluctuate by less than 4.00 Å, with no individual fluctuations over 6.00 Å for the entire duration of the 1 $\mu$s MD simulation in both the crystal structures and their derivative models (Figure 4). The above results suggest a controlled dynamic behavior in all systems, validating the native conformations observed in the experimental crystallographic structures.

Supplementary Movie S1 (crystal structure, 7TAM) illustrates that the conformation of the Y71 side chain remains stable, staying within H-bond distance from D54 for the entire duration of the simulations, thus keeping the SI/II pocket occluded; this occlusion is corroborated by the violin plots in Figure 5, which demonstrates a relatively fixed distance between D54-Y71, approximately equal to 3.1 Å for most of the simulated time in the three MD simulations of 7TAM. Supplementary Movie S2 (crystal structure, 4EFM) demonstrates that the side chain of Y71 tends to remain in the "flipped" conformation, never approaching D54 sufficiently to form an H-bond and keeping the distance over 7.0 Å to D54 (see MD_1 and MD_2 in Figure 5) most of the time; consequently, the SI/II pocket remains accessible. Supplementary Movie S3 (Model 1) and S4 (Model 2) demonstrate a conformational change in the Y71 side chain within the initial 250 ns of simulation. In Model 1, Y71 flips away from D54, increasing the mean distance between residues from the initial H-bond distance to approximately 12 Å, thus opening the SI/II pocket (MD_1 of Model 1 in Figure 5). In Model 2, an opposite conformational change is observed: Y71 flips toward D54, reducing the mean distance between atoms from approximately 13 Å down to 3 Å (a behavior more evident in MD_3 of Model 2 in Figure 5 but also a trend in MD_1 and MD_2) allowing the formation of an H-bond and thus occluding native accessibility of the SI/II pocket. Supplementary Movies S5 (Model 3 - HRas$^{Wild}$-GDP-bound) and S6 (Model 4 - HRas$^{Wild}$-GTP-bound) show results similar to 7TAM and 4EFM (Figure 5). However, the increased mobility of Switches I and II is reflected by an alternation of the SI/II pocket between the occluded and accessible forms (Figure 5 and Movie S5). This result suggests that the mutation tends to "freeze" the SI/II pocket in the accessible form since a similar alternating behavior was not observed for GppNHp-bound HRas$^{G12V}$ (Model 1), supporting prior findings which have shown that common Ras mutations can maintain the protein in a continuously active state.[8,9]

The conformational behavior of HRas observed for the duration of the MD simulations (Supplementary Movies S1−S6) suggests that the movement of the Y71 side chain toward D54 is correlated to the conformational state of the SI region upon GDP binding to HRas. In contrast, the "flipped" conformation of Y71 is observed upon GppNHp binding to HRas, where Y71 adopts a recessed position away from D54. The SI region gains conformational flexibility in the GppNHp-bound form of HRas yet remains relatively stable in the GDP-bound form of HRas. These conformational dynamics are reflected in the RMSF plots shown in Figure 4, which highlight the deviation of the SI region's position within 3D space over the duration of the MD simulations. In the case of experimental structure 7TAM, the maximum spatial deviation of SI was below


https://doi.org/10.1021/acsomega.4c10493
ACS Omega 2025, 10, 9463−9473

**Table 3. H-Bonds Formed between Tyr71 and other HRas Residues during the MD Simulations[a]**

| System | Interacting protein residues | | |
|---|---|---|---|
| | MD_1 | MD_2 | MD_3 |
| 7TAM (GDP) | $Y71_{SC}$–$D54_{SC}$ (80.60%) | $Y71_{SC}$–$D54_{SC}$ (61.69%) | $Y71_{SC}$–$D54_{SC}$ (79.10%) |
| | $Y71_{MC}$–$M67_{MC}$ (43.28%) | $Y71_{MC}$–$M67_{MC}$ (87.06%) | $Y71_{MC}$–$M67_{MC}$ (60.20%) |
| 4EFM (GppNHp) | $Y71_{MC}$–$M67_{MC}$ (23.38%) | $Y71_{MC}$–$M67_{MC}$ (34.33%) | $Y71_{MC}$–$M67_{MC}$ (32.84%) |
| | | $Y71_{SC}$–$E37_{SC}$ (21.39%) | $Y71_{SC}$–$L6_{MC}$ (52.74%) |
| Model 1 (GppNHp) | $Y71_{SC}$–$D54_{SC}$ (87.06%) | $Y71_{MC}$–$M67_{MC}$ (51.74%) | $Y71_{SC}$–$D54_{SC}$ (83.08% |
| | $Y71_{MC}$–$M67_{MC}$ (42.79%) | $Y71_{SC}$–$D38_{SC}$ (53.73%) | $Y71_{MC}$–$M67_{MC}$ (71.64%) |
| Model 2 (GDP) | $Y71_{MC}$–$M67_{MC}$ (21.50%) | $Y71_{MC}$–$M67_{MC}$ (17.91%) | $Y71_{MC}$–$M67_{MC}$ (37.81%) |
| | $Y71_{SC}$–$L6_{MC}$ (47.50%) | $Y71_{SC}$–$S39_{SC}$ (11.44%) | |
| | $Y71_{SC}$–$D54_{SC}$ (10.50%) | | |
| Model 3 (GTP) | $Y71_{SC}$–$D54_{SC}$(65.67%) | $Y71_{SC}$–$D54_{SC}$(69.65%) | $Y71_{SC}$–$D54_{SC}$(65.67%) |
| | $Y71_{MC}$–$M67_{MC}$(40.30%) | $Y71_{MC}$–$M67_{MC}$(41.29%) | $Y71_{MC}$–$M67_{MC}$(34.33%) |
| Model 4 (GDP) | $Y71_{SC}$–$D54_{SC}$(80.60%) | $Y71_{SC}$–$D54_{SC}$(61.69%) | $Y71_{SC}$–$D54_{SC}$(79.10%) |
| | $Y71_{MC}$–$M67_{MC}$(43.28%) | $Y71_{MC}$–$M67_{MC}$(87.06%) | $Y71_{MC}$–$M67_{MC}$(60.20%) |

[a]Only the residues capable of forming H-bonds with Tyr71 for over 10% of the simulated time are shown. SC = Side Chain; MC = Main Chain.

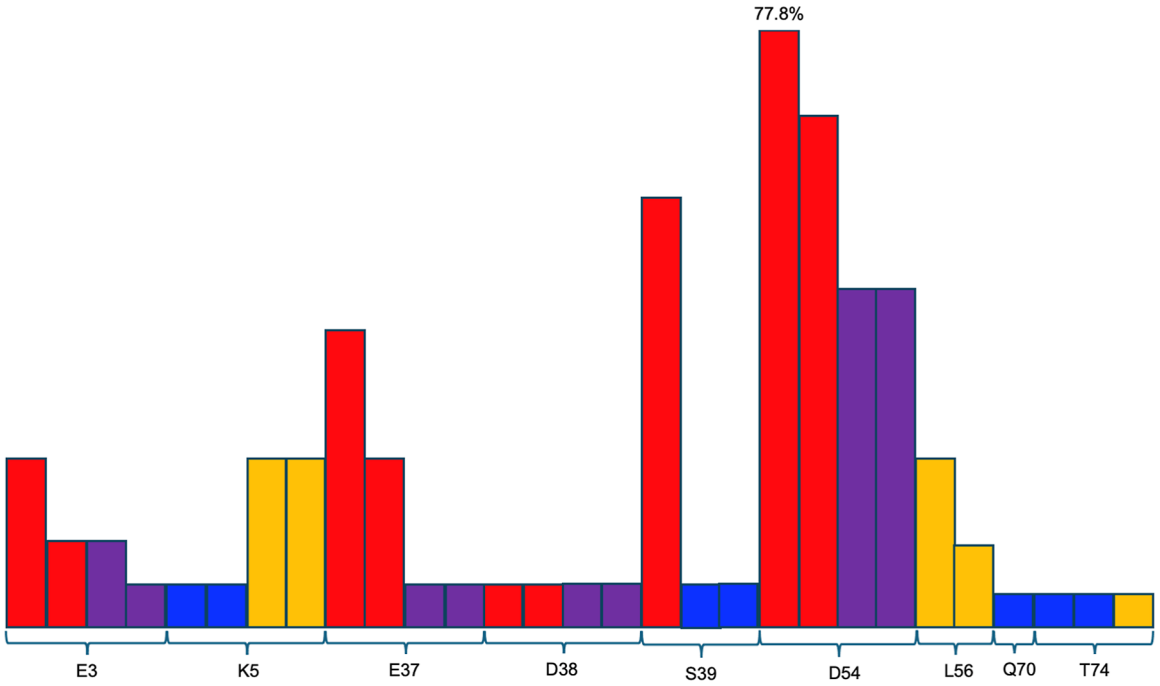


**Figure 6.** Fingerprints of the strong interactions on the SI/II pocket of the Ras experimental structures available in the PDB (www.rcsb.org). Color bars code: Red = backbone H-bond acceptor; blue = backbone H-bond donor; purple = ionic attraction; orange = arene attraction.

4 Å in all simulations (Figure 4A). In contrast, for experimental structure 4EFM, the maximum spatial deviation of the SI region was approximately 6 Å (Figure 4A). The fluctuations observed for SII were generally below or around 4 Å for all systems except 4EFM, where a maximum fluctuation close to 6 Å was observed. The heightened fluctuations of SII in4EFM can be correlated to the movement of the $\alpha$2 helix and the subsequent deviation of Y71. The plots for the synthetic models show average RMSF fluctuations below 4 Å for the entire duration of the MD simulations (Figure 4B,C). In Models 1 and 3, the movement of SI pushes Y71 away from D54, rendering the SI/II pocket occluded and accessible in an alternating fashion. In Models 2 and 4, an opposite motion for Y71 is observed: the side chain of Y71 exits the "flipped" conformation and extends to create an H-bond with D54, occluding the SI/II pocket. In the synthetic models, the changes forced on the SI/II pocket region are generally undone during the MD simulations, suggesting that native access to the SI/II pocket is stable in both the GDP and GppNHp-bound forms of HRas. Typically, native access to the SI/II pocket occurs only in the GppNHp/GTP-bound form of the protein. This rule (Figure S4) is consistent with most HRas/Ras structures published to the PDB and counteracts outlier structures (e.g., PDB ID: 6MQT) where this observation does not hold. To the best of our knowledge, most Ras-GppNHp-bound protein structures available in the PDB present an accessible SI/II pocket, while most Ras-GDP-bound structures present an occluded pocket. A true inference of the biological relevance of this rule would require a study of the conformational dynamics of the SI/II pocket on a time scale relevant to ligand binding (several milliseconds to several seconds). Although the orientations of Y71 and D54 appear consistent throughout the millisecond time frame of the conducted MD simulations, extended simulations are required to attain true consensus regarding the rule established above, the likes of


https://doi.org/10.1021/acsomega.4c10493
ACS Omega 2025, 10, 9463−9473

which are yet difficult to achieve using modern computing resources.

Analysis of Table 2 reveals that, as expected, the same residues appear to modulate nucleotide interactions in all systems studied. A notable exception is G13, which creates supplemental interactions with the bound GppNHp nucleotide, forming multiple H-bonds as a donor and receptor. These supplemental moderate−strength interactions are achieved through the supplemental $-NPO_3$ group of GppNHp, which results in the nucleotide occupying a larger volume of the HRas nucleotide binding pocket. We believe this key G13$-NPO_3$ interaction minimizes the separation between the p-loop and the bound nucleotide, causing a downstream cascade effect that results in the flipping of the Y71 side chain and thus bypassing SI/II pocket occlusion. Additionally, Table 3 reveals that Y71, aside from principally interacting with D54, most often creates H-bond interactions with M67 in all systems, as observed in experimental PDB structure 4EFM, as well as Model 1 and Model 2. In these systems, Y71 also creates additional H-bonds with L6, E37, D38, and S39. This result corroborates the flipping of Y71 to interact with the side chain of M67 as discussed in the crystallographic structure investigation above (see Results section).

Analysis of the fingerprints in Figure 6 reveal that H-bonds, ionic, and arene attractions with D54, S39 and Lys5 are the most frequent among the SI/II pocket binders, while H-bonds and arene attractions with L56, Q70 and T74 play a secondary role. Notably, H-bonds and ionic attractions with the neighboring residues E3, E37 and D38 appear relevant for ligand stabilization. These results allow us to point to those residues as key docking residues for the design of potential pan-Ras ligands.

## CONCLUSION

Our study presents the first complete native structure of GDP-bound $HRas^{G12V}$ (PDB ID: 7TAM): this experimental structure reveals an H-bond interaction between D54 and Y71, impeding native access to the inside surface of the SI/II pocket. Further MD simulations conducted using our published structure, together with the use of an experimental structure of GppNHp-bound $HRas^{G12V}$ and four synthetic models derived from each experimental structure, reveal that the association between D54 and Y71 is linked to the dynamic behavior of switches SI and SII, which are in turn influenced by the binding of either GDP or GTP to the nucleotide pocket. Upon GDP binding, it was observed that the side chain of Y71 sits in-plane with D54, leading to SI/II pocket occlusion. In contrast, GTP binding causes Y71 to flip away from D54 toward a neighboring residue in the $\alpha$2 helix, M67, eliminating SI/II pocket occlusion. Our MD simulations suggest that the G12V mutation tends to "freeze" the SI/II pocket open relatively to $HRas^{Wild}$, corroborating the statement that Ras mutations typically lock the protein in an active signaling state.[8,9] Our findings, combined with other complementary studies focused on the dynamics of Ras and potential drug suitability of the Ras platform, can inform future structure-based drug design efforts to unlock new therapeutic interventions for a target that has long been of great interest to the scientific community.[40]

## ASSOCIATED CONTENT

### Data Availability Statement

Crystallographic data generated in this study are publicly available in the RCSB worldwide Protein DataBank (PDB) under the accession code 7TAM. Molecular dynamics data generated in this study are available within the article and its Supporting Information files.

### Supporting Information

The Supporting Information is available free of charge at https://pubs.acs.org/doi/10.1021/acsomega.4c10493.

Data refinement and collection statistics for $HRas^{G12V}$-GDP (Table S1); Ramachandran plots for $HRas^{G12V}$-GDP (Figure S1), Plots of variation of total energy (Figure S2); Plots of variation of RMSD (Figure S3); Plots of variation of SASA (Figure S4); Conformational dynamics of the switch II region and residue Y71 (Figure S5); Polder OMIT maps comprising residues within the SI/SII pocket region of 7TAM and 4EFM (Figure S6) (PDF)

Movie S1: Dynamical behavior of D54 and Y7 in 7TAM during a 1 $\mu$s of MD simulation (MPG)

Movie S2: Dynamical behavior of D54 and Y71 in 4EFM during a 1 $\mu$s of MD simulation (MPG)

Movie S3: Dynamical behavior of D54 and Y71 in Model 1 during a 1 $\mu$s of MD simulation (MPG)

Movie S4: Dynamical behavior of D54 and Y71 in Model 2 during a 1 $\mu$s of MD simulation (MPG)

Movie S5: Dynamical behavior of D54 and Y71 in Model 3 during a 1 $\mu$s of MD simulation (MPG)

Movie S6: Dynamical behavior of D54 and Y71 in Model 4 during a 1 $\mu$s of MD simulation (MPG)

## AUTHOR INFORMATION


### Corresponding Author

**Steven R. LaPlante** − *NMX Research and Solutions Inc., Laval, Québec H7 V 5B7, Canada; PROTEO, the Quebec Network for Research on Protein Function, Engineering, and Applications, Universite Laval, Quebec, QC G1V 0A6, Canada;* orcid.org/0000-0003-2835-5789; Email: Steven.LaPlante@inrs.ca

### Authors

**Tanos C. C. França** − *INRS Centre Armand Frappier Santé Biotechnologie, Laval, Quebec H7 V 1B7, Canada; Laboratory of Molecular Modeling Applied to the Chemical and Biological Defense (LMCBD), Military Institute of Engineering (IME), 22290-270 Rio de Janeiro, Brazil; Center for Basic and Applied Research, Faculty of Informatics and Management, University of Hradec Kralove, 50003 Hradec Kralove, Czech Republic;* orcid.org/0000-0002-6048-8103

**Michael Maddalena** − *Institut National de la Recherche Scientifique (INRS), Centre Armand-Frappier Sante Biotechnologie, Universite du Quebec, Institut Pasteur International Network, Laval, QC H7V 1B7, Canada; PROTEO, the Quebec Network for Research on Protein Function, Engineering, and Applications, Universite Laval, Quebec, QC G1V 0A6, Canada*

**Imène Kouidmi** − *Institut National de la Recherche Scientifique (INRS), Centre Armand-Frappier Sante Biotechnologie, Universite du Quebec, Institut Pasteur International Network, Laval, QC H7V 1B7, Canada; PROTEO, the Quebec Network for Research on Protein Function, Engineering, and Applications, Universite Laval, Quebec, QC G1V 0A6, Canada*

**Yann Ayotte** − *NMX Research and Solutions Inc., Laval, Québec H7 V 5B7, Canada*




https://doi.org/10.1021/acsomega.4c10493
ACS Omega 2025, 10, 9463−9473

**Salim T. Islam** − *Institut National de la Recherche Scientifique (INRS), Centre Armand-Frappier Sante Biotechnologie, Universite du Quebec, Institut Pasteur International Network, Laval, QC H7V 1B7, Canada; PROTEO, the Quebec Network for Research on Protein Function, Engineering, and Applications, Universite Laval, Quebec, QC G1V 0A6, Canada;* orcid.org/0000-0001-6853-8446

Complete contact information is available at: https://pubs.acs.org/10.1021/acsomega.4c10493

### Author Contributions

⊥T.C.C.F and M.M. contributed equally to this manuscript. T.C.C.F.: Conceptualization, Molecular modeling studies, Writing—original draft, Formal analysis, Writing—review and editing, Methodology.M.M.: Conceptualization, Crystallography studies, Writing—original draft, Formal analysis, Writing—review and editing, Methodology.Y.A.: Conceptualization, Writing—review and editing S.T.I.: Funding acquisition, Supervision, Writing—review and editing. S.L.: Conceptualization, Funding acquisition, Supervision, Writing—review and editing.I.K.: Crystallography studies, Formal analysis.

### Funding

Financial support −SynergiQc grant, Centre Québecois de Développement du Médicament consortium (to all); NMX Research Solutions Inc. (to Yann Ayotte), Mitacs Accelerate grant (to Tanos C. C. França)

### Notes

The authors declare the following competing financial interest(s): Yann Ayotte is an employee of NMX Research Solutions.

## ■ ACKNOWLEDGMENTS

The authors thank the Canadian Light Source facility for providing the beamtime necessary for the advancement of this project. We would also like to thank Calcul Québec for providing timeslots to perform out-of-house MD simulations on their supercomputer cluster. T.C.C.F. thanks the support of the project - Long-term development plan UHK.

## ■ REFERENCES

(1) Zenonos, K.; Kyprianou, K. RAS signaling pathways, mutations and their role in colorectal cancer. *World J. Gastrointest. Oncol.* **2013**, *5* (5), 97. (a) Downward, J. Ras signalling and apoptosis. *Curr. Opin. Genet. Dev.* **1998**, *8* (1), 49−54. (b) Downward, J. Targeting RAS signalling pathways in cancer therapy. *Nat. Rev. Cancer* **2003**, *3* (1), 11−22.

(2) Pylayeva-Gupta, Y.; Grabocka, E.; Bar-Sagi, D. RAS oncogenes: weaving a tumorigenic web. *Nat. Rev. Cancer* **2011**, *11* (11), 761−774.

(3) Prior, I. A.; Hood, F. E.; Hartley, J. L. The Frequency of Ras Mutations in CancerRas Cancer Statistics. *Cancer Res.* **2020**, *80* (14), 2969−2974.

(4) Prior, I. A.; Lewis, P. D.; Mattos, C. A comprehensive survey of Ras mutations in cancer. *Cancer Res.* **2012**, *72* (10), 2457−2467.

(5) (a) Larda, S. T.; Ayotte, Y.; Denk, M. M.; Coote, P.; Heffron, G.; Bendahan, D.; Shahout, F.; Girard, N.; Iddir, M.; Bouchard, P.; Bilodeau, F.; Woo, S.; Farmer, L. J.; LaPlante, S. R. A Robust Strategy for Hit-to-Lead Discovery: NMR for SAR. *J. Med. Chem.* **2023**, *66*, 13427. (b) Bendahan, D.; Franca, T. C. C.; Amiens, K.; Ayotte, Y.; Forgione, P.; LaPlante, S. Synthesis of a thiophene-based fluorinated library applied to fragment-based drug discovery via 19F NMR with confirmed binding to mutant HRASG12V. *New J. Chem.* **2024**, *48*, 17872−17877.

(6) Gasper, R.; Wittinghofer, F. The Ras switch in structural and historical perspective. *Biol. Chem.* **2019**, *401* (1), 143−163.

(7) Karouzaki, S.; Peta, C.; Tsirimonaki, E.; Mangoura, D. PKCε-dependent H-Ras activation encompasses the recruitment of the RasGEF SOS1 and of the RasGAP neurofibromin in the lipid rafts of embryonic neurons. *Neurochem. Int.* **2019**, *131*, 104582.

(8) Malumbres, M.; Barbacid, M. RAS oncogenes: the first 30 years. *Nat. Rev. Cancer* **2003**, *3* (6), 459−465.

(9) Wey, M.; Lee, J.; Jeong, S. S.; Kim, J.; Heo, J. Kinetic mechanisms of mutation-dependent Harvey Ras activation and their relevance for the development of Costello syndrome. *Biochemistry* **2013**, *52* (47), 8465−8479.

(10) Gremer, L.; Gilsbach, B.; Reza Ahmadian, M.; Wittinghofer, A. Fluoride complexes of oncogenic Ras mutants to study the Ras-RasGap interaction. *Biol. Chem.* **2008**, *389*, 1163−1171.

(11) Smith, M. J.; Neel, B. G.; Ikura, M. NMR-based functional profiling of RASopathies and oncogenic RAS mutations. *Proc. Natl. Acad. Sci. U.S.A.* **2013**, *110* (12), 4574−4579.

(12) (a) Muraoka, S.; Shima, F.; Araki, M.; Inoue, T.; Yoshimoto, A.; Ijiri, Y.; Seki, N.; Tamura, A.; Kumasaka, T.; Yamamoto, M.; et al. Crystal structures of the state 1 conformations of the GTP-bound H-Ras protein and its oncogenic G12V and Q61L mutants. *FEBS Lett.* **2012**, *586* (12), 1715−1718. (b) Shima, F.; Ijiri, Y.; Muraoka, S.; Liao, J.; Ye, M.; Araki, M.; Matsumoto, K.; Yamamoto, N.; Sugimoto, T.; Yoshikawa, Y.; et al. Structural basis for conformational dynamics of GTP-bound Ras protein. *J. Biol. Chem.* **2010**, *285* (29), 22696−22705.

(13) (a) Geyer, M.; Schweins, T.; Herrmann, C.; Prisner, T.; Wittinghofer, A.; Kalbitzer, H. R. Conformational transitions in p21 ras and in its complexes with the effector protein Raf-RBD and the GTPase activating protein GAP. *Biochemistry* **1996**, *35* (32), 10308−10320. (b) Cherfils, J.; Zeghouf, M. Regulation of small gtpases by gefs, gaps, and gdis. *Physiol. Rev.* **2013**, *93* (1), 269−309.

(14) (a) Zhang, M.; Jang, H.; Nussinov, R. The structural basis for Ras activation of PI3Kα lipid kinase. *Phys. Chem. Chem. Phys.* **2019**, *21* (22), 12021−12028. (b) Vo, U.; Vajpai, N.; Embrey, K. J.; Golovanov, A. P. Dynamic studies of H-Ras• GTPγS interactions with nucleotide exchange factor Sos reveal a transient ternary complex formation in solution. *Sci. Rep.* **2016**, *6* (1), 29706.

(15) (a) Spoerner, M.; Herrmann, C.; Vetter, I. R.; Kalbitzer, H. R.; Wittinghofer, A. Dynamic properties of the Ras switch I region and its importance for binding to effectors. *Proc. Natl. Acad. Sci. U.S.A.* **2001**, *98* (9), 4944−4949. (b) Kapoor, A.; Travesset, A. Differential dynamics of RAS isoforms in GDP-and GTP-bound states. *Proteins:Struct., Funct., Bioinf.* **2015**, *83* (6), 1091−1106. (c) Buhrman, G.; O'Connor, C.; Zerbe, B.; Kearney, B. M.; Napoleon, R.; Kovrigina, E. A.; Vajda, S.; Kozakov, D.; Kovrigin, E. L.; Mattos, C. Analysis of binding site hot spots on the surface of Ras GTPase. *J. Mol. Biol.* **2011**, *413* (4), 773−789. (d) O'Connor, C.; Kovrigin, E. L. Global conformational dynamics in ras. *Biochemistry* **2008**, *47* (39), 10244−10246.

(16) Lanfredini, S.; Thapa, A.; O'Neill, E. RAS in pancreatic cancer. *Biochem. Soc. Trans.* **2019**, *47* (4), 961−972.

(17) Rojas, A. M.; Fuentes, G.; Rausell, A.; Valencia, A. The Ras protein superfamily: evolutionary tree and role of conserved amino acids. *J. Cell Biol.* **2012**, *196* (2), 189−201.

(18) Kessler, D.; Bergner, A.; Böttcher, J.; Fischer, G.; Döbel, S.; Hinkel, M.; Müllauer, B.; Weiss-Puxbaum, A.; McConnell, D. B. Drugging all RAS isoforms with one pocket. *Future Med. Chem.* **2020**, *12* (21), 1911−1923.

(19) (a) Haza, K. Z.; Martin, H. L.; Rao, A.; Turner, A. L.; Saunders, S. E.; Petersen, B.; Tiede, C.; Tipping, K.; Tang, A. A.; Ajayi, M.; et al. RAS-inhibiting biologics identify and probe druggable pockets including an SII-α3 allosteric site. *Nat. Commun.* **2021**, *12* (1), 4045. (b) Pierre, S.; bats, A. S.; Coumoul, X. Understanding SOS (son of sevenless). *Biochem. Pharmacol.* **2011**, *82* (9), 1049−1056.

(20) Kessler, D.; Gmachl, M.; Mantoulidis, A.; Martin, L. J.; Zoephel, A.; Mayer, M.; Gollner, A.; Covini, D.; Fischer, S.; Gerstberger, T.; et al. Drugging an undruggable pocket on KRAS. *Proc. Natl. Acad. Sci. U.S.A.* **2019**, *116* (32), 15823−15829.

(21) Maurer, T.; Garrenton, L. S.; Oh, A.; Pitts, K.; Anderson, D. J.; Skelton, N. J.; Fauber, B. P.; Pan, B.; Malek, S.; Stokoe, D.; et al. Small-molecule ligands bind to a distinct pocket in Ras and inhibit SOS-

mediated nucleotide exchange activity. *Proc. Natl. Acad. Sci. U.S.A.* **2012**, *109* (14), 5299−5304.
(22) Sun, Q.; Burke, J. P.; Phan, J.; Burns, M. C.; Olejniczak, E. T.; Waterson, A. G.; Lee, T.; Rossanese, O. W.; Fesik, S. W. Discovery of small molecules that bind to K-Ras and inhibit Sos-mediated activation. *Angew. Chem., Int. Ed.* **2012**, *51* (25), 6140−6143.
(23) (a) Chen, F.-Y.; Li, X.; Zhu, H.-P.; Huang, W. Regulation of the ras-related signaling pathway by small molecules containing an indole core scaffold: A potential antitumor therapy. *Front. Pharmacol* **2020**, *11*, 280. (b) Larda, S. T.; Ayotte, Y.; Denk, M. M.; Coote, P.; Heffron, G.; Bendahan, D.; Shahout, F.; Girard, N.; Iddir, M.; Bouchard, P.; et al. Robust Strategy for Hit-to-Lead Discovery: NMR for SAR. *J. Med. Chem.* **2023**, *66*, 13416−13427.
(24) (a) Vonrhein, C.; Flensburg, C.; Keller, P.; Sharff, A.; Smart, O.; Paciorek, W.; Womack, T.; Bricogne, G. Data processing and analysis with the autoPROC toolbox. *Acta Crystallogr., Sect. D:Biol. Crystallogr.* **2011**, *67* (4), 293−302. (b) Kabsch, W. xds. *Acta Crystallogr., Sect. D:Biol. Crystallogr.* **2010**, *66* (2), 125−132. (c) Evans, P. R. An introduction to data reduction: space-group determination, scaling and intensity statistics. *Acta Crystallogr., Sect. D:Biol. Crystallogr.* **2011**, *67* (4), 282−292.
(25) Zwart, P. H.; Afonine, P. V.; Grosse-Kunstleve, R. W.; Hung, L.-W.; Ioerger, T. R.; McCoy, A. J.; McKee, E.; Moriarty, N. W.; Read, R. J.; Sacchettini, J. C. *Automated structure solution with the PHENIX suite*; Springer, 2008.
(26) (a) Emsley, P.; Lohkamp, B.; Scott, W. G.; Cowtan, K. Features and development of Coot. *Acta Crystallogr., Sect. D:Biol. Crystallogr.* **2010**, *66* (4), 486−501. (b) Afonine, P. V.; Grosse-Kunstleve, R. W.; Echols, N.; Headd, J. J.; Moriarty, N. W.; Mustyakimov, M.; Terwilliger, T. C.; Urzhumtsev, A.; Zwart, P. H.; Adams, P. D. Towards automated crystallographic structure refinement with phenix. refine. *Acta Crystallogr., Sect. D:Biol. Crystallogr.* **2012**, *68* (4), 352−367.
(27) Williams, C. J.; Headd, J. J.; Moriarty, N. W.; Prisant, M. G.; Videau, L. L.; Deis, L. N.; Verma, V.; Keedy, D. A.; Hintze, B. J.; Chen, V. B.; et al. MolProbity: More and better reference data for improved all-atom structure validation. *Protein Sci.* **2018**, *27* (1), 293−315.
(28) Case, D. A.; Darden, T.; Cheatham, T.; Simmerling, C. L.; Wang, J.; Duke, R. E.; Luo, R.; Crowley, M.; Walker, R. C.; Zhang, W. *Amber 10*; University of California, 2008.
(29) Nelson, M. T.; Humphrey, W.; Gursoy, A.; Dalke, A.; Kalé, L. V.; Skeel, R. D.; Schulten, K. NAMD: a parallel, object-oriented molecular dynamics program. *International Journal of Supercomputer Applications and High Performance Computing* **1996**, *10* (4), 251−268.
(30) (a) França, T. C.; Botelho, F. D.; Drummond, M. L.; LaPlante, S. R. Theoretical Investigation of Repurposed Drugs Potentially Capable of Binding to the Catalytic Site and the Secondary Binding Pocket of Subunit A of Ricin. *Acs Omega* **2022**, *7* (36), 32805−32815. (b) Franca, T. C. C.Goncalves, A. d. S.Bérubé, C.Voyer, N.Aubry, N.LaPlante, S. R.Determining the Predominant Conformations of Mortiamides A−D in Solution Using NMR Data and Molecular Modeling Tools*Acs Omega2023* (c) Vieira, L. A.; Almeida, J. S.; De Koning, M. C.; LaPlante, S. R.; Borges, I. Jr; França, T. C. Molecular modeling of Mannich phenols as reactivators of human acetylcholinesterase inhibited by A-series nerve agents. *Chem.-Biol. Interact.* **2023**, *382*, 110622. (d) França, T. C.; Saïdi, F.; Ajamian, A.; Islam, S. T.; LaPlante, S. R. Molecular Dynamics of Outer Membrane-Embedded Polysaccharide Secretion Porins Reveals Closed Resting-State Surface Gates Targetable by Virtual Fragment Screening for Drug Hotspot Identification. *Acs Omega* **2024**, *9*, 13226.
(31) (a) Ono, S.; Naylor, M. R.; Townsend, C. E.; Okumura, C.; Okada, O.; Lee, H.-W.; Lokey, R. S. Cyclosporin A: conformational complexity and chameleonicity. *J. Chem. Inf. Model.* **2021**, *61* (11), 5601−5613. (b) Hirano, M.; Toyota, K.; Ishibashi, H.; Tominaga, N.; Sato, T.; Tatarazako, N.; Iguchi, T. Molecular insights into structural and ligand binding features of methoprene-tolerant in daphnids. *Chem. Res. Toxicol.* **2020**, *33* (11), 2785−2792. (c) Ali, Z.; Cardoza, J. V.; Basak, S.; Narsaria, U.; Singh, V. P.; Isaac, S. P.; França, T. C. C.; LaPlante, S. R.; George, S. S. Computational design of candidate multi-epitope vaccine against SARS-CoV-2 targeting structural (S and N) and non-structural (NSP3 and NSP12) proteins. *J. Biomol. Struct. Dyn.* **2023**, *41*, 13348−13367.
(32) (a) Goga, N.; Rzepiela, A.; De Vries, A.; Marrink, S.; Berendsen, H. Efficient algorithms for Langevin and DPD dynamics. *J. Chem. Theory Comput.* **2012**, *8* (10), 3637−3649. (b) Izaguirre, J. A.; Catarello, D. P.; Wozniak, J. M.; Skeel, R. D. Langevin stabilization of molecular dynamics. *J. Chem. Phys.* **2001**, *114* (5), 2090−2098. (c) Lange, O. F.Grubmüller, H.Collective Langevin dynamics of conformational motions in proteins*J. Chem. Phys.***2006***124*21 (d) Stella, L.; Lorenz, C. D.; Kantorovich, L. Generalized Langevin equation: An efficient approach to nonequilibrium molecular dynamics of open systems. *Phys. Rev. B* **2014**, *89* (13), 134303. (e) Wu, X.; Brooks, B. R. Self-guided Langevin dynamics simulation method. *Chem. Phys. Lett.* **2003**, *381* (3−4), 512−518.
(33) Humphrey, W.; Dalke, A.; Schulten, K. VMD: visual molecular dynamics. *Graphics* **1996**, *14*, 33−38.
(34) Smith, R. H.; Dar, A. C.; Schlessinger, A. PyVOL: a PyMOL plugin for visualization, comparison, and volume calculation of drug-binding sites. *BioRxiv* **2019**, 816702.
(35) (a) DeLano, W. L. *Pymol: An open-source molecular graphics tool*. CCP4 Newsl. Protein Crystallogr. 2002, *40*(1), 82−92. (b) DeLano, W. L.; Bromberg, S. *PyMOL user's guide*; DeLano Scientific LLC; Vol. *2004*, p 629.
(36) Kalbitzer, H. R.; Spoerner, M. State 1 (T) inhibitors of activated Ras. *enzymes* **2013**, *33*, 69−94.
(37) Moore, A. R.; Rosenberg, S. C.; McCormick, F.; Malek, S. RAS-targeted therapies: is the undruggable drugged? *Nat. Rev. Drug Discovery* **2020**, *19* (8), 533−552.
(38) (a) Kessler, D.; Gollner, A.; Gmachl, M.; Mantoulidis, A.; Martin, L. J.; Zoephel, A.; Mayer, M.; Covini, D.; Fischer, S.; Gerstberger, T.; Gmaschitz, T.; et al. Reply to Tran et al.: Dimeric KRAS protein−protein interaction stabilizers. *Proc. Natl. Acad. Sci. U.S.A.* **2020**, *117* (7), 3365−3367.
(39) (a) Ingólfsson, H. I.; Neale, C.; Carpenter, T. S.; Shrestha, R.; López, C. A.; Tran, T. H.; Oppelstrup, T.; Bhatia, H.; Stanton, L. G.; Zhang, X.; et al. Machine learning−driven multiscale modeling reveals lipid-dependent dynamics of RAS signaling proteins. *Proc. Natl. Acad. Sci. U.S.A.* **2022**, *119* (1), No. e2113297119. (b) Rudack, T.; Teuber, C.; Scherlo, M.; Güldenhaupt, J.; Schartner, J.; Lübben, M.; Klare, J.; Gerwert, K.; Kötting, C. The Ras dimer structure. *Chem. Sci.* **2021**, *12* (23), 8178−8189. (c) Simanshu, D. K.; Philips, M. R.; Hancock, J. F. Consensus on the RAS dimerization hypothesis: Strong evidence for lipid-mediated clustering but not for G-domain-mediated interactions. *Mol. Cell* **2023**, *83* (8), 1210−1215.
(40) (a) Parker, M. I.; Meyer, J. E.; Golemis, E. A.; Dunbrack, R. L. Delineating the RAS Conformational Landscape. *Cancer Res.* **2022**, *82* (13), 2485−2498. (b) Wang, H.; Liu, D.; Yu, Y.; Fang, M.; Gu, X.; Long, D. Exploring the state- and allele-specific conformational landscapes of Ras: understanding their respective druggabilities. *Phys. Chem. Chem. Phys.* **2023**, *25* (2), 1045−1053.


https://doi.org/10.1021/acsomega.4c10493
*ACS Omega* 2025, 10, 9463−9473